Proceedings of the Institute of Acoustics

EXPERIMENTALLY-TUNED SYNTHESIS OF A THIN PLATE

S Duran Department of Industrial Engineering, University of Bologna, Italy
M Ducceschi Department of Industrial Engineering, University of Bologna, Italy
H Tahvanainen Department of Industrial Engineering, University of Bologna, Italy
L Ausiello SENE, University of Portsmouth, Portsmouth, Hampshire, UK

1 INTRODUCTION

The numerical simulation of acoustic instruments and devices is a growing subject of research.[1] Applications range from model-aided instrument making,[2–5] to virtual instrument and effect design,[6–9] to virtual reality applications.[10,11] A faithful reproduction of the underlying system may be realised via signal-based analysis and resynthesis,[12] starting usually from a recorded sample. Model-based synthesis,[6,13] on the other hand, allows to reproduce the dynamics of common objects such as strings, bars and plates by setting a few physically meaningful parameters feeding a mathematical model. The latter allows far greater flexibility in terms of control and design, but often lacks the realism of the former. This work investigates the possibility of tuning a physical model using experimental data. The system considered here is a cantilever metal plate struck with a hammer. The physical model is derived from a modal decomposition of the Kirchhoff plate equation.[14] A preliminary estimate of the unknown plate's rigidity constant is carried out first, via the measurement of the first eigenfrequency. Then, the finite difference scheme is used to solve the eigenvalue problem over a fine grid with the computed rigidity constant, and the modal shapes are then stored along with the modal frequencies. Experimental data are collected from a laboratory experiment, and a comparison of the experimental frequencies against the model's eigenfrequencies is carried out. The modal equations obtained from the difference scheme are then adjusted to compensate for the errors in the eigenfrequencies. Experimental decay times are also implemented in the scheme. Tuned numerical impulse responses at three different combinations of input and output locations are then computed and compared to the experimental responses, showing a high degree of accuracy.

The paper is organised as follows. Section 2 presents the thin plate equation, as well as the finite difference scheme used to obtain the numerical eigenbasis of a cantilever plate. Section 3 details the experimental setup to obtain the plate's frequencies and decay times. Finally, in Section 4 the output spectra of the finite difference scheme are compared against the experimental ones.

2 MODELS

The Kirchhoff equation provides a model for the dynamics of a thin plate. In the presence of losses and sources, this is:

$$\rho L_z \frac{\partial^2 u(\mathbf{x},t)}{\partial t^2} = -D\Delta\Delta u(\mathbf{x},t) - 2\rho L_z \sigma \frac{\partial u(\mathbf{x},t)}{\partial t} + \delta(\mathbf{x}-\mathbf{x}_f) f(t). \tag{1}$$

In the above, $u : \mathbb{R}^2 \times \mathbb{R} \to \mathbb{R}$ is the displacement of the plate, a function of the Cartesian coordinates $\mathbf{x} = (x, y) \in \mathcal{V} := [0, L_x] \times [0, L_y]$ as well as time $t \geq 0$. Constants appear as: ρ, the volume density of the plate; L_x, L_y, L_z, the dimensions of the plate along x, y and z, with $L_z \ll L_x, L_y$; σ, a loss factor; D, the rigidity of the plate, defined as:

$$D := \frac{EL_z^3}{12(1-\nu^2)}, \tag{2}$$

where E is Young's modulus, and ν is Poisson's ratio. Furthermore, $\Delta\Delta$ is the biharmonic operator, and $f(t)$ is an external input acting pointwise at $\mathbf{x}_f$.

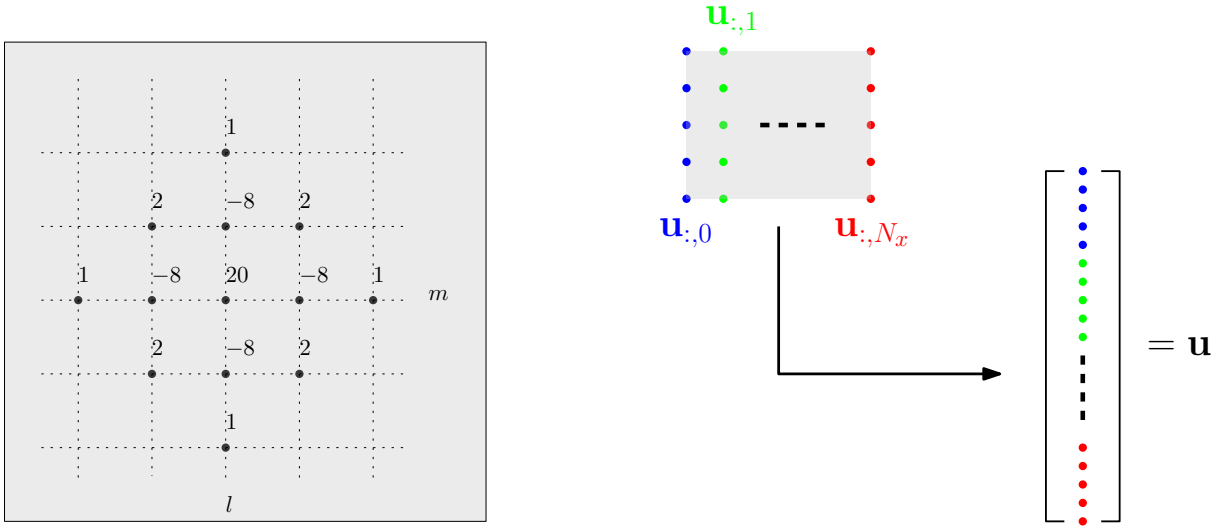

Figure 1: Left: representation of the biharmonic coefficients at the internal grid point (l, m) (all coefficients are scaled by h^{-4}). Right: the creation of the state vector $\mathbf{u}(t)$ by stacking consecutive strips of grid points.

The model is completed by a set of suitable boundary conditions, given here for the cantilever case; that is, a free plate with one clamped edge. Thus:

$$u = \partial_x u = 0 \quad \text{at } \{y = 0, x \in [0, L_x]\}, \tag{3a}$$

$$\frac{\partial^3 u}{\partial \eta^3} + (2-\nu)\frac{\partial^3 u}{\partial \eta \partial \tau^2} = \frac{\partial^2 u}{\partial \eta^2} + \nu \frac{\partial^2 u}{\partial \tau^2} = 0 \quad \text{at } \{y = L_y, x \in [0, L_x]\} \cup \{x = \{0, L_x\}, y \in [0, L_y]\}, \tag{3b}$$

where η, τ denote the perpendicular and tangential directions to the boundary, respectively.

2.1 Spatial Discretisation

A solution to (1) will be sought in the modal domain. The modes are not available in closed-form for the cantilever case, and will thus be obtained by solving a numerical eigenvalue problem. To that end, consider a finite difference approximation of the displacement: the continuous function $u(\mathbf{x}, t)$ is approximated by a grid function $u_{l,m}(t)$, at the grid locations (lh, mh), where $0 \leq l \leq N_x$, $0 \leq m \leq N_y$ and where h is the grid spacing. Thus, the problem is discretised on a $(N_x + 1) \times (N_y + 1)$ grid of points.

It is convenient to stack strips of points, so that the $u_{l,m}(t)$ becomes the column vector $\mathbf{u}(t)$ of length $(N_x + 1)(N_y + 1)$. Thus, the continuous biharmonic operator $\Delta\Delta$ is approximated by a matrix $\mathbf{B}$ of dimensions $(N_x + 1)(N_y + 1) \times (N_x + 1)(N_y + 1)$, see Figure 1 for a pictorial representation. The delta function in (1) becomes itself a vector via Lagrange interpolation, denoted here $\mathbf{J}$, see Bilbao.[6] The semi-discrete Kirchhoff equation, thus, becomes:

$$\rho L_z \ddot{\mathbf{u}} = -D\mathbf{B}\mathbf{u} - 2\rho L_z \sigma \dot{\mathbf{u}} + \mathbf{J}(\mathbf{x}_f) f(t). \tag{4}$$

One has:

$$\mathbf{B} := \mathbf{Q}\mathbf{\Lambda}\mathbf{Q}^{-1}, \tag{5}$$

where $\mathbf{Q}$ is the matrix of numerical eigenvectors, and $\mathbf{\Lambda}$ is a positive diagonal matrix of eigenvalues.

Hence, left-multiplying the above by $\mathbf{Q}^{-1}/\rho L_z$ yields:

$$\ddot{\mathbf{U}} = -\mathbf{\Omega}^2 \mathbf{U} - 2\mathbf{C}\dot{\mathbf{U}} + \frac{1}{\rho L_z}\mathbf{Q}^{-1}\mathbf{J} f(t), \tag{6}$$

where $\mathbf{U} := \mathbf{Q}^{-1}\mathbf{u}$ is here a vector of modal coordinates, $[\mathbf{\Omega}]_{p,p} := \frac{D}{\rho L_z}[\sqrt{\mathbf{\Lambda}}]_{p,p} := \omega_p$ is a diagonal matrix of eigenfrequencies, and $\mathbf{C}$ is a diagonal matrix of loss coefficients, $[\mathbf{C}]_{p,p} := \sigma_p$, replacing the global damping coefficient σ in (1). These are related to the more common decay times $\tau^{(60)}$ by:

$$\sigma_p := 3\log(10)\left(\tau_p^{(60)}\right)^{-1}. \tag{7}$$

Here, $\tau^{(60)}$ denotes the 60 dB decay time. The modal system above is completely diagonal, as expected for a linear problem. In this work, the damping ratios σ_p and the resonant frequencies ω_p will be obtained experimentally, and the output of the modal system (6) will be computed and compared to the experimental results. Since impulse response will be considered, one may set $f(t) := \delta(t - t_0)$.

Once the time evolution of the modal coordinates is computed, one may reconstruct the physical output at the desired location $\mathbf{x}_o$ via:

$$u(\mathbf{x}_o, t) = h^2 \mathbf{J}^\intercal(\mathbf{x}_o) \mathbf{Q}\, \mathbf{U}(t). \tag{8}$$

2.2 Time discretisation

System (6) can be integrated in time using the leapfrog scheme.[6] To that end, the continuous-time vector $\mathbf{U}(t)$ is approximated by a vector time series $\mathbf{U}^n$, at the time $t_n := kn$, with $n \in \mathbb{N}$ being the time index, and k being the time step (the multiplicative inverse of the sample rate; for audio, this is usually set as $k = 1/44100$). The scheme used here is thus:

$$(\mathbf{I} + k\mathbf{C})\mathbf{U}^{n+1} = \left(2\mathbf{I} - k^2\mathbf{\Omega}^2\right)\mathbf{U}^n + (-\mathbf{I} + k\mathbf{C})\mathbf{U}^{n-1} + \frac{k^2}{\rho L_z}\mathbf{Q}^{-1}\mathbf{J}(\mathbf{x}_f) f^n, \tag{9}$$

where $\mathbf{I}$ is the identity matrix. Since $\mathbf{C}$ is diagonal, the scheme is fully explicit. A stability condition arises as $k < 2/\max(\omega_p)$, which is verified for the cases considered below.

3 MODAL ANALYSIS AND EVALUATION

The modal system (6) is expressed in terms of the geometrical and material parameters, as well as the eigenfrequencies ω_p and damping ratios σ_p, where $1 \leq p \leq N$ (N here indicates the total number of modes retained in the simulations). The geometrical parameters L_x, L_y, L_z, as well as the density ρ can be measured trivially from the experimental plate, and are listed in Figure 3. The rigidity D is unknown. This will be estimated from a vibroacoustic measurement of the plate's first eigenfrequency, as detailed below.

3.1 Experimental Setup

To implement the desired boundary conditions, a simple clamping structure is built in accordance with previous research.[15] To fix the plate to the base structure, two angular hinges are clamped to each other, acting as the main clamping system. An additional steel rectangular flat bar is also used with a layer of rubber material to help distribute the pressure along the angular elements' entire length and along the plate's bottom clamped side, approximating the clamped boundary condition (3a). A miniature impact hammer is used to excite the plate, while a single axial piezoelectric accelerometer measures the structure's impulse response (IR), as shown in figure 2. The cantilever plate's dimensions and known physical properties are reported in Figure 3.

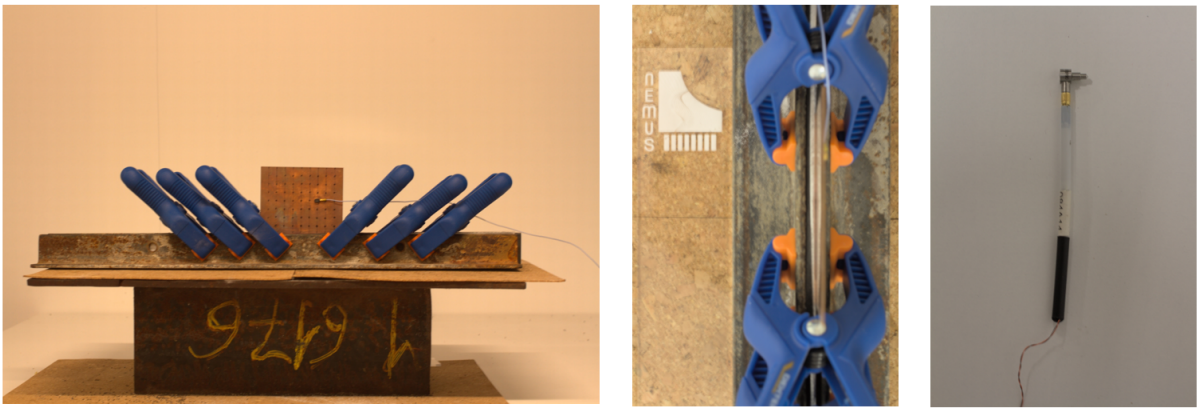

Figure 2: Left: Front view of the experimental setup. Centre: Top view of the experimental setup. Right: Miniature impact hammer used to excite the plate.

To acquire the data, the impact hammer roves over 3 different positions across the plate surface's area while the accelerometer is mounted on a single surface point, as sketched in Figure 3. The collected data is then post-processed in Matlab and the natural frequencies of the system are detected from the frequency response functions

(FRFs) with the use of Matlab's own peak finding routine, thus effectively measuring the ω_p's over the range of interest, here restricted to the range $0 \leq \omega \leq 2000\pi$ (i.e. only frequencies up to 1 kHz were here considered). The same routine is used to extract the half-power bandwidth of the peaks, from which an estimate of the loss coefficients σ_p's is obtained.[16]

To reduce measurement uncertainty due to the low repeatability of the impact hammer force signal, 10 different IRs were averaged over each measurement point, resulting in a total of 3 averaged IRs.[16] Finally, Chladni patterns were implemented experimentally to observe the plate nodal lines over the thin plate surface.[17] To do so, a miniature shaker was used to excite the cantilever plate and white sand was placed over the plate's surface. Pure tone signals having the same frequencies as the first six measured peaks in the analyzed FRFs were used as excitation signals.

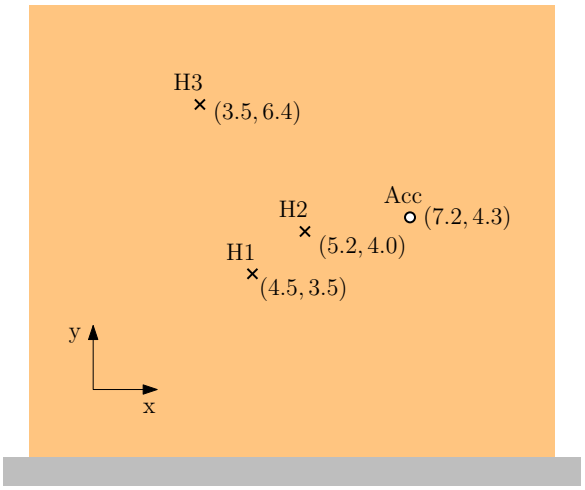

Plate parameters

L_x (cm)	L_y (cm)	L_z (mm)	ρ (kg · m^{-3})
10	8	0.81	8765

Figure 3: The cantilever plate, impact hammer (Hx) and accelerometer measurement positions considered in the study. Measurements locations are reported as (x, y) coordinates on the plate surface, in cm. The plate's known parameters are also indicated. The rigidity D is estimated as per the method described in Section 3.2.

3.2 Estimate of the rigidity constant from measurements

The first cantilever mode is a "flapping" mode with no dependence along x, see Figure 4. Thus, the first cantilever plate eigenfrequency may be written as:

$$\omega_1^2 = \frac{D\pi^4}{\rho L_z L_y^4}\alpha. \tag{10}$$

where α is a non-dimensional parameter, constant for all plates sharing the same aspect ratio. α may be estimated easily from the finite difference scheme above. For that, run a few simulations with a sufficiently fine grid, changing the material and geometrical parameters (but keeping the aspect ratio $L_y L_x^{-1} = 4/5$, as per the experimental plate in Figure 3), and compute α using (10). This indeed shows that:

$$\alpha \approx 0.13 \tag{11}$$

for all the plates considered in this test. Hence, an estimate of the rigidity constant for the experimental plate is obtained immediately by inverting (10), using the value of α above and the experimentally measured eigenfrequency $f_1 = 73.2$ Hz. This gives:

$$D \approx 4.86 \text{ N} \cdot \text{m} \implies E \approx 100 \text{ GPa}, \tag{12}$$

in line with tabulated values for brass alloys.[18]

3.3 Assessment of the results

The numerical and the experimental frequencies identified from the spatially averaged FRFs are compared in Table 1, showing a very good match with the exception of the fourth eigenfrequency, displaying a larger deviation. The same table reports the numerical result from a FEM simulation in COMSOL, yielding eigenfrequencies very close to the FD scheme. On average, a deviation of 2.7% is obtained by comparing the experimental and numerical frequencies. Such value is lower than the final errors reported in similar studies comparing experimental and

FEM data for rectangular enclosures,[19] thus confirming the reliability of the thin plate model employed here. Furthermore, the current analysis confirms the reliability of the α estimation method reported in Section 3.2. A visual comparison of the numerical and experimental mode shapes is given in Figure 4, showing a good agreement.

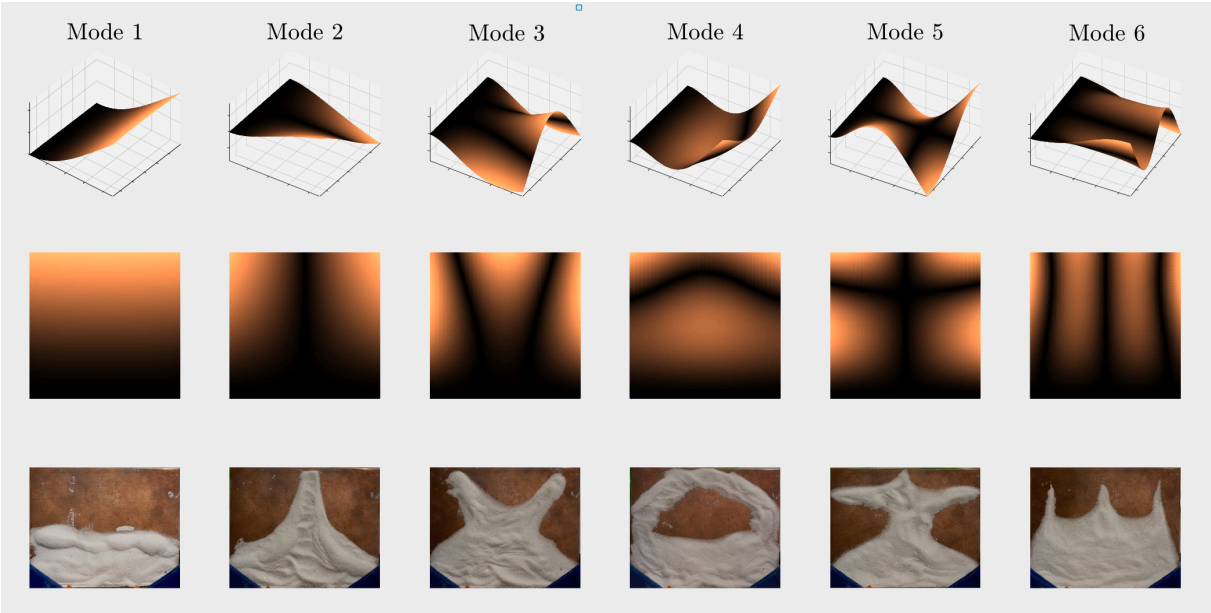

Figure 4: Numerical and experimental mode shapes. Top row: 3D view of the numerical modal shapes; middle row: top view of the numerical mode shapes; bottom row: experimental Chladni patterns showing the nodal lines.

	Eigenfrequency (Hz)						
	1	2	3	4	5	6	*Average*
FD (proposed)	72	149.7	381.6	459.5	577.5	888.9	–
FEM (COMSOL)	71.6	148.6	379.1	456.7	572.9	883.8	–
Experimental	73.2	148	376	431	559	910	–
Deviation FD-Exp. (%)	1.6	1.1	1.5	6.2	3.2	2.4	2.7

Table 1: Numerical and experimental eigenfrequencies. The finite difference scheme is run using a grid spacing $h = 10^{-3}\sqrt{L_x L_y} \approx 8.9 \cdot 10^{-5}$, yielding $N_x = 1118$, $N_y = 894$. The COMSOL simulation is run using the predefined "extremely fine" mesh size.

4 SIMULATION RESULTS

Figure 5 reports the results of the simulations in the frequency range of interest up to 910 Hz. The three subplots report the acceleration spectra of the output of the finite difference scheme, compared against the experimental spectra, for the three input positions (H1,H2,H3) reported in Figure 3. Each subplot presents four curves: the experimental (solid black); the FD scheme with constant loss coefficient $\sigma = 17.3$ (dashed blue); the frequency-adjusted FD scheme with constant loss coefficient $\sigma = 17.3$ (dashed red); the frequency-adjusted FD scheme with tuned loss coefficients σ_p (solid yellow). Note that here the spectra are obtained from the dynamical model of the plate equation, as per (1), and are not the result of a "best fit" such as via the PolyMAX algorithm.[20] For all cases, a clear improvement is obtained by adjusting the eigenvalues $\mathbf{\Omega}$ in (6), and further improvements are obtained by adjusting the decay times. The adjusted frequencies are as per Table 1 (*Experimental*), whilst the tuned decay times are as per $\tau^{(60)} = [0.8, 0.4, 0.6, 0.3, 0.4, 0.5]$.

The good agreement of the tuned FD scheme with the experimental curves suggests that the proposed method could be used to improve the accuracy of model-based synthesis, though a more thorough comparison, including synthesised sound samples, is required to assess the method further.

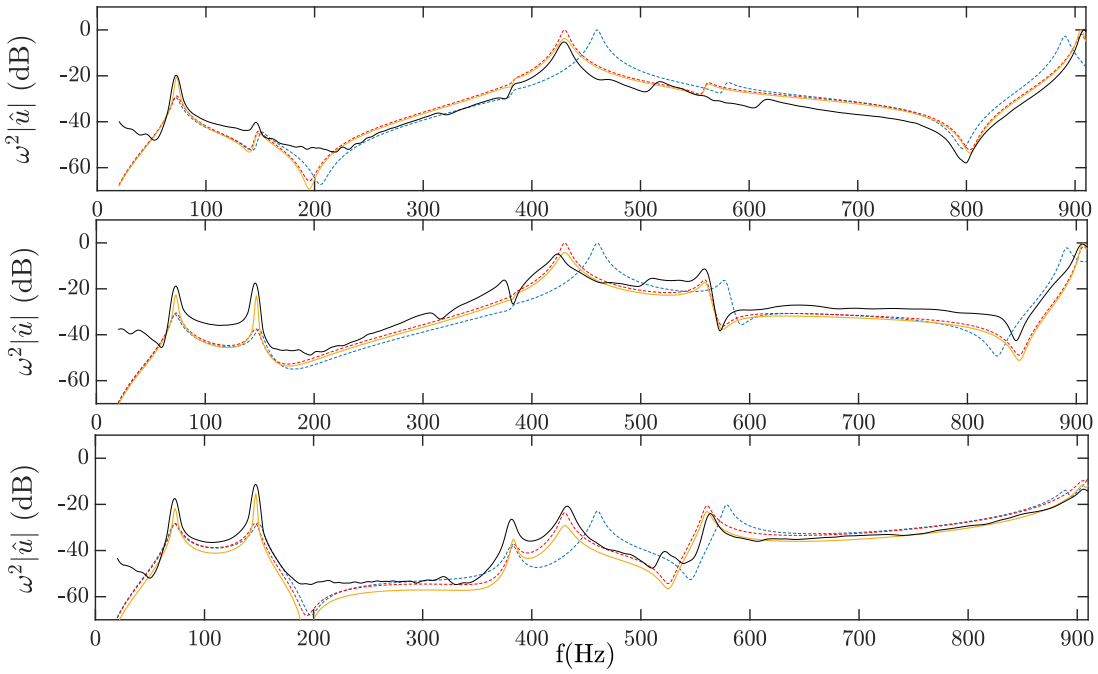

Figure 5: Output acceleration spectra of the proposed finite difference scheme, and the experimental spectra. Colour scheme: black (experimental); blue and dashed (FD scheme, constant σ); red and dashed (frequency-adjusted FD scheme, constant σ); yellow (frequency-adjusted FD scheme, tuned σ_p's). The spectra have been normalised so to take a maximum value of 1 across the plotted range. Top panel: $H1$; middle panel: $H2$; bottom panel: $H3$.

5 CONCLUSIONS

This work explored the possibility of improving the accuracy of model-based synthesis by adjusting the numerical eigenvalues of a finite difference approximation of the Kirchhoff plate equation. For that, modal analysis was performed on an experimental plate in order to recover the plate's frequencies and decay times. Then, the Kirchhoff plate equations were discretised on a numerically-computed modal basis, and simulations were run with and without frequency correction. Whilst the original numerical eigenfrequencies do show good agreement with the experimental ones, a much better match is obtained by correcting the eigenfrequencies. Further improvements are obtained by adjusting the decay times, which may be easily set mode by mode in this framework. These results suggest that it is possible to retain the flexibility of model-based sound synthesis, whilst improving its accuracy by carefully selecting the modal parameters. Further investigations are underway to provide a more extensive comparison across the whole audible spectrum.

Acknowledgements

This work received funding from the European Research Council (ERC) under the Horizon2020 framework, grant number 950084-StG-NEMUS. HT's work has been supported by the Finnish Cultural Foundation.

6 REFERENCES

[1] N. Giordano and V. Chatziioannou. Status and future of modeling of musical instruments: Introduction to the jasa special issue. *The Journal of the Acoustical Society of America*, 150(3):2294–2301, 2021.

[2] T. Yoshinaga, H. Yokoyama, T. Shoji, A. Miki, and A. Iida. Global numerical simulation of fluid-structure-acoustic interaction in a single-reed instrument. *The Journal of the Acoustical Society of America*, 149(3):1623–1632, 2021.

[3] H. Tahvanainen, H. Matsuda, and R. Shinoda. Numerical simulation of the acoustic guitar in virtual prototyping. Detmold, Germany, 2019.

[4] S. Gonzalez, D. Salvi, F. Antonacci, and A. Sarti. Eigenfrequency optimisation of free violin plates. *The Journal of the Acoustical Society of America*, 149(3):1400–1410, 2021.

[5] Jean-Théo Jiolat, Christophe d'Alessandro, Jean-Loïc Le Carrou, and José Antunes. Toward a physical model of the clavichord. *The Journal of the Acoustical Society of America*, 150(4):2350–2363, 2021.

[6] Stefan Bilbao. *Numerical sound synthesis: finite difference schemes and simulation in musical acoustics*. John Wiley & Sons, 2009.

[7] C.J. Webb and S. Bilbao. On the limits of real-time physical modelling synthesis with a modular environment. In *Proceedings of the 18th International Conference on Digital Audio Effects (DAFx15)*, Trondheim, Norway, 2015.

[8] M. Ducceschi, S. Bilbao, and C.J. Webb. Real-time modal synthesis of nonlinearly interconnected networks. In *Proceedings of the 26th International Conference on Digital Audio Effects (DAFx23)*, Copenhagen, Denmark, 2023.

[9] M. Ducceschi and C. J Webb. Plate reverberation: Towards the development of a real-time physical model for the working musician. In *Proceedings of the 22nd International Congress on Acoustics (ICA-16)*, Buenos Aires, Argentina, 2016.

[10] M. Karjalainen and T. Maki-Patola. Physics-based modeling of musical instruments for interactive virtual reality. In *IEEE 6th Workshop on Multimedia Signal Processing, 2004.*, pages 223–226. IEEE, 2004.

[11] S. Serafin, S. Gelineck, N. Böttcher, and L. Martinussen. Virtual reality instruments capable of changing physical dimensions in real-time. In *Enactive 2005*. 2005.

[12] X. Serra. A system for sound analysis/transformation/synthesis based on a deterministic plus stochastic decomposition. Master's thesis, Stanford University, 1989.

[13] J.O. Smith. *Physical Audio Signal Processing, online book, 2010 edition*. W3K Publishing, 2010.

[14] M. Géradin and D. J. Rixen. *Mechanical vibrations: theory and application to structural dynamics*. John Wiley & Sons, 2014.

[15] C. Warren, C. Niezrecki, P. Avitabile, and P. Pingle. Comparison of frf measurements and mode shapes determined using optically image based, laser, and accelerometer measurements. *Mechanical Systems and Signal Processing*, 25(6):2191–2202, 2011.

[16] P. Avitabile. *Modal testing: a practitioner's guide*. John Wiley & Sons, 2017.

[17] PH Tuan, CP Wen, PY Chiang, YT Yu, Hsing-Chin Liang, Kai-Feng Huang, and Yung-Fu Chen. Exploring the resonant vibration of thin plates: Reconstruction of chladni patterns and determination of resonant wave numbers. *The Journal of the Acoustical Society of America*, 137(4):2113–2123, 2015.

[18] William D Callister Jr. *Materials science and engineering an introduction*. John Wiley & Sons, 2007.

[19] S. Mohamady, R. K. Raja Ahmad, A. Montazeri, R. Zahari, and Nawal Aswan Abdul Jalil. Modeling and eigenfrequency analysis of sound-structure interaction in a rectangular enclosure with finite element method. *Advances in Acoustics and Vibration*, 2009(6):2191–2202, 2009.

[20] B. Peeters, H. Van der Auweraer, P. Guillaume, and J. Leuridan. The polymax frequency-domain method: a new standard for modal parameter estimation? *Shock and Vibration*, 11(3-4):395–409, 2004.